Nonunitary quantum trajectory Monte Carlo method for open quantum systems

Marek Seliger,[1] Carlos O. Reinhold,[2,3] Tatsuya Minami,[2,3] and Joachim Burgdörfer[1,3]
[1]*Institute for Theoretical Physics, Vienna University of Technology, A-1040 Vienna, Austria, EU*
[2]*Physics Division, Oak Ridge National Laboratory, Oak Ridge, Tennessee 37831-6372, USA*
[3]*Department of Physics and Astronomy, University of Tennessee, Knoxville, Tennessee 37996-1200, USA*
(Received 15 October 2004; published 15 June 2005)

We have developed a generalized nonunitary Lindblad equation and its quantum trajectory Monte Carlo implementation for the evolution of open quantum systems (OQSs) whose coupling to the environment features not only energy exchange but also probability flux to the environment. This generalization allows the treatment of a class of problems where the state space of the system includes bound and continuum states. We show the equivalence between the solution of the generalized Lindblad equation and the Monte Carlo average over open quantum trajectories. As a first test case we study the multilevel radiative decay of a hydrogenic ion. As a second test case we apply the theory to the time development of the internal state of fast highly charged Kr^{35+} ions traversing carbon foils with varying thickness subject to collisions and to spontaneous radiative decay. We find significantly improved agreement of the nonunitary transport theory with experimental data.

DOI: 10.1103/PhysRevA.71.062901 PACS number(s): 34.50.Fa, 34.10.+x

I. INTRODUCTION

The open quantum system (OQS) approach provides a useful theoretical framework for describing the time evolution of a system interacting with an environment representing a large number of degrees of freedom. The underlying concept of studying the partially coherent dynamics of the reduced "small" system under the influence of all other degrees of freedom of the problem to be traced out is at the core of investigations of decoherence. For example, the coupling between an atom (the small system) and the vacuum fluctuations of the radiation field (the environment) results in spontaneous transitions in the atomic system (i.e., radiative decay) and thus to decoherence as well as in modifications of the eigenstates by shifting their eigenenergies (the Lamb shift).

The starting point of a theoretical analysis of OQSs is, typically, the reduction of the master equation for the reduced density matrix to a Redfield equation by applying the Born-Markov approximation [1–5]. Even with such a drastic simplification which treats the coupling to the environment in first-order perturbation theory and neglects memory effects, solution of the equation of motion for the density is still a formidable task. Difficulties in describing OQSs in terms of the evolution of the reduced density matrix have their source in the high dimensionality of the problem. In the solution of the master equation for the reduced density matrix (N^2) of the N-state system, N^4 couplings are involved. The OQS approach was first successful for the theoretical description of atomic systems involving only few states [1,3]. However, many problems in atomic physics require a high-dimensional state space for which the N^4 scaling makes a direct solution of the underlying master equation impracticable.

The importance of the quantum trajectory Monte Carlo (QTMC) method [4,5] and closely related techniques such as the Monte Carlo wave-function method [1–3] lie in the reduction of dimensionality. Propagating states rather than the density operators leads to a scaling with N^2 while controlling the statistical error of the result by introducing another scaling with the number of trajectories.

Solving the Redfield equation by QTMC techniques requires its reduction to a form strictly preserving positive definiteness of the reduced density matrix. This can be conveniently achieved by a reduction to a Lindblad form [6,7]. Alternatively, a solution of the Redfield equation by QTMC methods has been proposed [8,9] requiring, however, an extended state space. Depending on the physical system to be described, the reduction to the Lindblad form is not unique and is still an open problem. We have recently introduced a form for this reduction that accounts for both the buildup of coherences as well as the decoherence [5]. Our analysis was motivated by experimental studies of collisionally induced coherences in highly charged Kr^q ($q=35$) ions traversing carbon foils at high speeds ($v_p=47$ a.u.).

The passage of an atomic system through solids under multiple-scattering conditions provides a classic example of the interaction of an open quantum system (the projectile) with a large environment (the solid). Studying such transport problems has the advantage that the system-environment interaction is switched on suddenly when the projectile enters the solid and ceases suddenly after escaping from the solid, thus allowing the time-resolved study of the evolution of the density matrix on an attosecond to femtosecond time scale. While good agreement was found for thin foils corresponding to short times, discrepancies for larger distances ($\geqslant 10^4$ a.u.) corresponding to propagation times of $\geqslant 5$ fs were observed [5]. These discrepancies were particularly troubling as they only appeared within the formulation of quantum transport in terms of a Lindblad equation [5] while with an earlier more phenomenological model [10] better agreement was found. Understanding and resolving these discrepancies is the aim of this paper.

One key feature of the Lindblad equation is the unitarity of the evolution of the reduced system described, built in by construction. The point to be noted is that preservation of

positivity does not necessarily require unitarity. In fact, the unitarity of Lindblad equation is of limited value when dealing with any truncated Hilbert space of the reduced system in a realistic simulation. As flux out of this subspace into its complement can and, in general, is bound to occur, enforced unitarity means unphysical suppression of flux and thus distortion of the evolution within the truncated Hilbert space. A classic example is the propagation of wave packets of continuum electrons. Within any basis expansion or finite elements (grid) representation of finite dimension, only a bounded region in coordinate space can be represented. The wave packet will therefore be artificially reflected at the boundary unless absorbing boundary conditions, optical potentials, or masking functions are introduced [11]. All of these methods result in absorption of probability flux and thus in a manifestly nonunitary evolution. In analogy, we introduce in this paper a generalized nonunitary Lindblad equation and its QTMC realization that accounts for probability flux out of the truncated Hilbert space to be explicitly treated. The open quantum systems discussed in the following are not only open with respect to energy transfer but also with respect to probability flux. This change of approach can be viewed as the analogue to the transition from a canonical to a grand canonical ensemble in statistical mechanics. In the application to the projectile state evolution in the solid, the present approach permits us to treat explicitly the low-lying states of the ion within a finite Hilbert space of a size manageable within a numerical solution using a Monte Carlo method, while implicitly accounting for the flow of probability towards highly excited bound states and continuum states in the complement.

The plan of this paper is as follows: we briefly review the open quantum system approach and the solution by means of a quantum trajectory Monte Carlo method in Sec. II. In Sec. III we present our extension for nonunitary systems and illustrate its application for the simple test case of the radiative decay of a hydrogenic atom. In Sec. IV we apply our extension to the transport of hydrogenic atoms through solids and show that previously observed discrepancies can be accounted for. Atomic units ($|e|=m_e=\hbar=1, c=137$) will be used unless otherwise stated.

II. OPEN QUANTUM SYSTEM APPROACH FOR UNITARY SYSTEMS

In this section we briefly review the basic properties of the Lindblad equation and its solution by a quantum trajectory Monte Carlo method. A more detailed description can be found in Ref. [5]. Consider a system (S) of interest with Hamiltonian H_S interacting with an environment referred to in the following as reservoir (R) with Hamiltonian H_R through a coupling interaction V_{SR} [Fig. 1(a)]. The time evolution of the density matrix $\rho(t)$ of the entire interacting system is given by the Liouville–von Neumann equation

$$\frac{d}{dt}\rho(t) = -i[H,\rho(t)], \tag{2.1}$$

including the total Hamiltonian $H=H_S+H_R+V_{SR}$.

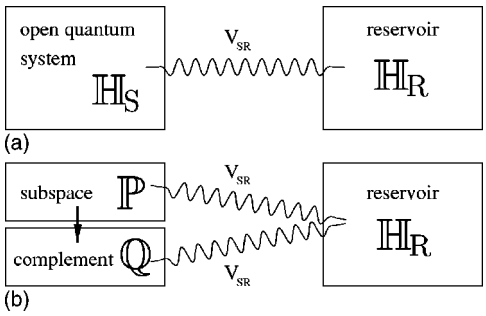

FIG. 1. Schematic picture of the open quantum system $\mathbb{H}_S$ interacting with the reservoir $\mathbb{H}_R$ via the interaction V_{SR}. (a) Full system $\mathbb{H}_S$ and (b) decomposition into subspace $\mathbb{P}$ and complement $\mathbb{P}$.

Clearly, the solution of the full Liouville–von Neumann equation is out of reach for realistic systems involving a large number of degrees of freedom. Instead, the focus is on a master equation, an equation of motion for the reduced density matrix of the system of interest $\sigma(t)$, which is obtained by tracing out all degrees of freedom of the reservoir by $\sigma(t)=\mathrm{Tr}_R[\rho(t)]$. One requirement for the reservoir is that it has a large number of degrees of freedom compared to those of the system such that the energy spacing of reservoir states is much smaller than that of the system providing a continuous excitation spectrum. The reduction entails usually a number of additional approximations such as the Born-Markov approximation which neglects memory effects, treats the coupling V_{SR} to first-order perturbation theory, and yields a master equation of the Redfield type [5]. A useful further reduction is the Lindblad equation [6,7]

$$\frac{d}{dt}\sigma(t) = -i[H_S,\sigma(t)] + R\sigma(t) \tag{2.2}$$

with the relaxation superoperator

$$R\sigma(t) = -\frac{1}{2V}\sum_{\vec{k}} [S^\dagger(\vec{k})S(\vec{k})\sigma(t) + \sigma(t)S^\dagger(\vec{k})S(\vec{k}) - 2S(\vec{k})\sigma(t)S^\dagger(\vec{k})], \tag{2.3}$$

that describes the interaction of the system with the reservoir and involves a sum containing the transition operator $S(\vec{k})$. The transition operator represents transitions between states of $\mathbb{H}_S$ due to the coupling with the reservoir determined by V_{SR}. The physical meaning of the summation label $\vec{k}$ and volume V depends on the system under consideration. In the following $\vec{k}$ represents the wave-number vector of the momentum exchange between system and reservoir but may also include polarization indices, etc. The time evolution of the reduced density matrix $\sigma(t)$ in this formalism is governed by H_S, the part of the total Hamiltonian acting on the system solely, and by the Lindblad transition operator $S(\vec{k})$. With this decomposition we separate the description of the dynamics into an unperturbed part of the small system without an environment (H_S) and put all effects of the presence of an environment (i.e., driving transitions within the open quantum system) into the relaxation superoperator (R). In the

quantum Monte Carlo trajectory realization the first term of Eq. (2.2) and the first two terms of Eq. (2.3) of the Lindblad master equation result in a continuous time evolution while the last terms in Eq. (2.3) is responsible for discontinuous ("jump") processes. Built into Eq. (2.2) is the strict positivity of $\sigma(t)$ for all times, i.e., $\sigma_{ii}(t) \geqslant 0$ for all i and t. The Lindblad equation describes an open quantum system (OQS) allowing for energy exchange

$$\frac{d}{dt}\langle H_S\rangle = \frac{d}{dt}\mathrm{Tr}[\sigma(t)H_S] \neq 0 \tag{2.4}$$

while preserving the total probability

$$\frac{d}{dt}\mathrm{Tr}_S[\sigma(t)] = 0. \tag{2.5}$$

The latter follows from the explicitly built-in unitarity of the evolution into the relaxation operator [Eq. (2.3)]. Equation (2.2) describes a unitary mapping of the Hilbert space of the system, $\mathbb{H}_S$, onto itself.

The popularity of the Lindblad equation is, in part, due to the fact that it can be mapped onto a nonlinear stochastic Schrödinger equation (NLSSE) without further assumptions or approximations. The advantage of such a mapping is that the NLSSE can be solved by propagating a Monte Carlo ensemble of state vectors: i.e., using the quantum trajectory Monte Carlo (QTMC) or Monte Carlo wave-function (MCWF) methods. In analogy to classical statistical mechanics, where the Boltzmann equation can be solved using test particle discretization following the trajectories of an ensemble of test particles in time, the Lindblad form of the master equation can be solved by an ensemble of quantum trajectories. The conceptual difference between quantum and classical trajectory Monte Carlo methods is that the dynamics of the classical trajectories in phase space is governed by the Langevin equation while in the quantum version each realization corresponds to a stochastically propagated state vector (quantum "trajectory" in Hilbert space) according the NLSSE.

Within the QTMC method the density matrix of a pure state is obtained as

$$\sigma(t) = \frac{1}{N_{traj}}\sum_{\eta=1}^{N_{traj}} |\Psi^\eta(t)\rangle\langle\Psi^\eta(t)|, \tag{2.6}$$

where N_{traj} is the number of quantum trajectories controlling the statistical uncertainty. In the limit $N_{traj}\to\infty$, the ensemble average can be shown to be strictly equivalent to the solution of the original Lindblad equation [12]. The time evolution of each trajectory is governed by the NLSSE,

$$|d\Psi^\eta(t)\rangle = \left[-iH_S\,dt - \frac{dt}{2V}\sum_{\vec{k}} [S^\dagger(\vec{k})S(\vec{k}) - \langle S^\dagger(\vec{k})S(\vec{k})\rangle_{t,\eta}] + \frac{1}{V}\sum_{\vec{k}} dN_{\vec{k}}^\eta(t)\left(\frac{S(\vec{k})}{\sqrt{\langle S^\dagger(\vec{k})S(\vec{k})\rangle_{t,\eta}}} - 1\right)\right]|\Psi^\eta(t)\rangle, \tag{2.7}$$

containing a stochastic element in the form of an Ito differential $dN_{\vec{k}}^\eta(t)$ that is 1 when a transition happens in an infinitesimal time interval dt and that is zero otherwise. This stochastic element generates different stochastic realizations of quantum trajectories labeled by η. It can be shown [12] that the reduced density matrix calculated as the Monte Carlo average (2.6) yields the Lindblad equation (2.2) when the expectation value of the Ito differentials for the system in state $|\Psi^\eta\rangle$ at time t are chosen as

$$\overline{dN_{\vec{k}}^\eta(t)dN_{\vec{k}'}^\eta(t)} = \overline{dN_{\vec{k}}^\eta(t)}\,\delta_{\vec{k}\vec{k}'} = dt\langle S^\dagger(\vec{k})S(\vec{k})\rangle_{t,\eta}\delta_{\vec{k}\vec{k}'}. \tag{2.8}$$

Solving the NLSSE the time evolution of each quantum trajectory is constructed by applying the time evolution operator onto the initial wave function as $|\Psi^\eta(t)\rangle = U^\eta(t,0)|\Psi^\eta(0)\rangle$. The time evolution operator $U^\eta(t,0)$ is constructed as a sequence of continuous time evolution operators and discontinuous jump operators as

$$U^\eta(t,0) = U_{cont}^\eta(t,t_n)\prod_{j=1}^{n} U_{jump}^\eta(\vec{k}_j,t_j)U_{cont}^\eta(t_j,t_{j-1}) \tag{2.9}$$

with $t_0=0$. The application of the continuous time evolution operator results in

$$|\Psi^\eta(t_j)\rangle = U_{cont}^\eta(t_j,t_{j-1})|\Psi^\eta(t_{j-1})\rangle = \frac{e^{-iH_{eff}(t_j-t_{j-1})}|\Psi^\eta(t_{j-1})\rangle}{||e^{-iH_{eff}(t_j-t_{j-1})}|\Psi^\eta(t_{j-1})\rangle||}, \tag{2.10}$$

with the effective Hamiltonian

$$H_{eff} = H_S - \frac{i}{2V}\sum_{\vec{k}} S^\dagger(\vec{k})S(\vec{k}) \tag{2.11}$$

including the unperturbed atomic Hamiltonian of the system (H_S) and the modification of the eigenstates due to the presence of the environment making the effective Hamiltonian non-Hermitian.

The discontinuous transitions

$$|\Psi^\eta(t_j+\delta t)\rangle = U_{jump}^\eta(\vec{k}_j,t_j)|\Psi^\eta(t_j)\rangle = \frac{S(\vec{k}_j)|\Psi^\eta(t_j)\rangle}{||S(\vec{k}_j)|\Psi^\eta(t_j)\rangle||} \tag{2.12}$$

are specified by a transition time (jump time) t_j and the parameter $\vec{k}_j$ which are determined by the coupling to the reservoir degrees of freedom. In spite of the non-Hermitian nature of H_{eff}, the evolution [Eqs. (2.10)–(2.12)] remains unitary as the renormalization of the kets [Eqs. (2.10) and (2.12)] restores the norm at each step.

III. NONUNITARY LINDBLAD EQUATION AND NLSSE

The unitarity constraint, Eq. (2.5), built into the Lindblad equation poses a hurdle for realistic numerical simulations as it remains in force when the Hilbert space is truncated to dimension N. For realistic high, but finite, dimensional systems which include continuum states a strictly unitary evolution is unphysical. Only a subspace $\mathbb{P}$ of the Hilbert space

$\mathbb{H}_S$ can be represented in a numerical simulation by a truncated basis of dimension N [see Fig. 1(b)]. The subspace $\mathbb{P}$ is coupled to its complement $\mathbb{Q}$ by the system-reservoir interaction V_{SR}. The flow of probability between $\mathbb{P}$ and $\mathbb{Q}$ is therefore not an artifact but real for any computationally feasible truncated basis set. The point to be noted is that $\mathbb{Q}$ refers to a subspace of the system Hilbert space, not to the reservoir [see Fig. 1(b)]. The interaction with the environment does not only drive transitions within the open quantum system $\mathbb{P}$, but is also responsible for probability flux out of it into $\mathbb{Q}$. Therefore the class of open quantum systems this approach can describe is not only open with respect to energy dissipation but also with respect to probability flux. In practice, numerical simulations take this effect into account by optical potentials or masking functions [11]. Their purpose is to prevent "reflection" of wave packets, i.e., the artificial confinement within $\mathbb{P}$ rather than the flow into $\mathbb{Q}$. Such approximations can account for a flow from $\mathbb{P}$ into $\mathbb{Q}$ while neglecting the backcoupling from $\mathbb{Q}$ to $\mathbb{P}$. Their consequence is the violation of unitarity within $\mathbb{P}\subset\mathbb{H}_S$. In the application to the excited-state evolution in the solid (see Sec. IV), $\mathbb{P}$ will represent the hydrogenic bound-state space up to $n\leqslant n_c$ where the cutoff quantum number is typically $n_c\approx 6$. (The dimension of $\mathbb{P}$ is then $N=182$.) Accordingly, $\mathbb{Q}$ represents higher-lying bound states ($n>6$) and the continuum spectrum of ionized electrons. Our goal is now to go beyond the restriction (2.5) and to develop a different master equation that accounts for the probability flow from $\mathbb{P}$ into $\mathbb{Q}$. To this end we introduce a generalized Lindblad equation $d\sigma(t)/dt=-i[H_S,\sigma(t)]+R^{NU}\sigma(t)$, in which the relaxation superoperator is replaced by its nonunitary (NU) version

$$R^{NU}\sigma(t) = -\frac{1}{2V}\sum_{\vec{k}}\left[P^{\mathrm{P}}S^{\dagger}(\vec{k})S(\vec{k})P^{\mathrm{P}}\sigma(t)+\sigma(t)P^{\mathrm{P}}S^{\dagger}(\vec{k})S(\vec{k})P^{\mathrm{P}} - 2S^{\mathrm{P}}(\vec{k})\sigma(t)S^{\mathrm{P}\dagger}(\vec{k})\right]. \tag{3.1}$$

In Eq. (3.1) S is defined in the entire Hilbert space $\mathbb{H}_S$ while S^{P} is the submatrix of S mapping $\mathbb{P}$ onto itself. That is, $S^{\mathrm{P}}=P^{\mathrm{P}}SP^{\mathrm{P}}$, where $P^{\mathrm{P}}=\Sigma_{\alpha\in\mathbb{P}}|\alpha\rangle\langle\alpha|$ is the projector operator onto the subspace $\mathbb{P}$. This gives rise to the decomposition

$$\Gamma^{\mathrm{PP}} = \frac{1}{V}\sum_{\vec{k}} S^{\mathrm{P}\dagger}(\vec{k})S^{\mathrm{P}}(\vec{k}) = \frac{1}{V}\sum_{\vec{k}}\Gamma^{\mathrm{PP}}(\vec{k}), \tag{3.2a}$$

$$\Gamma^{\mathrm{P}} = \frac{1}{V}\sum_{\vec{k}} P^{\mathrm{P}}S^{\dagger}(\vec{k})S(\vec{k})P^{\mathrm{P}} = \frac{1}{V}\sum_{\vec{k}}\Gamma^{\mathrm{P}}(\vec{k}), \tag{3.2b}$$

where the former describes the decay matrix within $\mathbb{P}$ while the latter also includes the decay from $\mathbb{P}$ to $\mathbb{Q}$. In other words, Eq. (3.2b) involves the submatrix $S^{\mathrm{PQ}}(\vec{k})$ mapping $\mathbb{P}$ onto $\mathbb{Q}$. Consequently the norm of $\sigma(t)$ is no longer conserved but decays according to

$$\frac{d}{dt}\mathrm{Tr}_{\mathrm{S}}[\sigma(t)] = -\mathrm{Tr}_{\mathrm{S}}[\Gamma^{\mathrm{P}}\sigma(t)]+\mathrm{Tr}_{\mathrm{S}}[\Gamma^{\mathrm{PP}}\sigma(t)] = -\frac{1}{V}\sum_{\vec{k}}\sum_{\alpha,\beta\in\mathbb{P}}\sum_{\nu\in\mathbb{Q}} S^{\dagger}_{\alpha\nu}(\vec{k})S_{\nu\beta}(\vec{k})\sigma_{\beta\alpha}, \tag{3.3}$$

where $S^{\dagger}_{\alpha\nu}$ and $S_{\nu\beta}$ in this equation correspond only to matrix elements of the submatrix S^{PQ}.

While general master equations that feature nonconservation of probability (or particle number) are well known, the specific novel aspect of the present formulation is that it can be mapped onto a wave-function propagation algorithm. This nonunitary extension of the Lindblad equation has the advantageous feature that the positive-definiteness requirement remains satisfied within $\mathbb{P}$. Consequently it can be solved using a QTMC algorithm as well, provided that a modified NLSSE and generalized versions of the continuous and jump operators,

$$|\Psi^{\eta}(t_j)\rangle = U^{\eta}_{cont}(t_j,t_{j-1})|\Psi^{\eta}(t_{j-1})\rangle = \||\Psi^{\eta}(t_{j-1})\rangle\|\frac{e^{-iH^{\mathrm{P}}_{eff}(t_j-t_{j-1})}|\Psi^{\eta}(t_{j-1})\rangle}{\|e^{-iH^{\mathrm{PP}}_{eff}(t_j-t_{j-1})}|\Psi^{\eta}(t_{j-1})\rangle\|}, \tag{3.4}$$

$$|\Psi^{\eta}(t_j+\delta t)\rangle = U^{\eta}_{jump}(\vec{k}_j,t_j)|\Psi^{\eta}(t_j)\rangle = \||\Psi^{\eta}(t_{j-1})\rangle\|\frac{S^{\mathrm{P}}(\vec{k}_j)|\Psi^{\eta}(t_j)\rangle}{\|S^{\mathrm{P}}(\vec{k}_j)|\Psi^{\eta}(t_j)\rangle\|}, \tag{3.5}$$

are applied. The non-Hermitian effective Hamiltonians entering Eq. (3.4) are

$$H^{\mathrm{P}}_{eff}=H_S-\frac{i}{2}\Gamma^{\mathrm{P}} \text{ and } H^{\mathrm{PP}}_{eff}=H_S-\frac{i}{2}\Gamma^{\mathrm{PP}}. \tag{3.6}$$

In contrast to Eq. (2.10), the continuous operator (3.4) does not preserve the norm of the wave function. The non-Hermitian Hamiltonians in Eq. (3.6) including the decay operators Γ^{P} and Γ^{PP} result in a nonunitary evolution in U^{η}_{cont} in Eq. (3.4). In the unitary QTMC method discussed in the previous section U^{η}_{cont} in Eq. (2.10) contains the same effective Hamiltonian in the nominator and in the denominator, resulting in an overall rotation of the state vector $|\Psi^{\eta}(t)\rangle$ in the Hilbert space $\mathbb{H}_S$. In the nonunitary QTMC method the effective Hamiltonians in U^{η}_{cont} differ by the sum over all S^{PQ}, which is the amount of coupling from $\mathbb{P}$ to the complement $\mathbb{Q}$. Consequently, U^{η}_{cont} in Eq. (3.4) accounts for the probability decrease in the subspace $\mathbb{P}$ due to flux into the complement $\mathbb{Q}$.

The corresponding NLSSE now becomes

$$|d\Psi^{\eta}(t)\rangle = \left\{-iH^{\mathrm{P}}_S\,dt-\frac{dt}{2}(\Gamma^{\mathrm{P}}-\langle\Gamma^{\mathrm{PP}}\rangle_{t,\eta}) + \frac{1}{V}\sum_{\vec{k}} dN^{\eta}_{\vec{k}}(t)\left(\frac{S^{\mathrm{P}}(\vec{k})}{\sqrt{\langle\Gamma^{\mathrm{PP}}(\vec{k})\rangle_{t,\eta}}}-1\right)\right\}|\Psi^{\eta}\rangle, \tag{3.7}$$

where the expectation values are now defined as $\langle\Gamma^{\mathrm{PP}}\rangle_{\eta}$

$=\langle\Psi^{\eta}|\Gamma^{\mathrm{PP}}|\Psi^{\eta}\rangle/\langle\Psi^{\eta}|\Psi^{\eta}\rangle$. In order to yield the generalized Lindblad form (3.1), the expectation value of the Ito differentials when the system is in state $|\Psi^{\eta}\rangle$ at time t is chosen as

$$\overline{dN_{\vec{k}}^{\eta}dN_{\vec{k}'}^{\eta}} = \overline{dN_{\vec{k}}^{\eta}(t)}\,\delta_{\vec{k}\vec{k}'} = dt\langle\Gamma^{\mathrm{PP}}(\vec{k})\rangle_{t,\eta}\delta_{\vec{k}\vec{k}'}. \tag{3.8}$$

In this case, the jump times can be obtained from the implicit equation

$$u = \frac{1}{\|\Psi^{\eta}(t_{j-1})\|^2}(1 - \|e^{-iH_{eff}^{\mathrm{PP}}(t_j - t_{j-1})}|\Psi^{\eta}(t_{j-1})\rangle\|^2), \tag{3.9}$$

where u is a uniformly distributed random number, $u \in [0,1]$.

In the Appendix we show the correspondence between the QTMC method and the generalized Lindblad master equation (3.1). We conclude this section by illustrating the significance and accuracy of the nonunitary QTMC method with the help of an exactly solvable model problem: the multilevel time evolution of an excited hydrogenic atom subject to spontaneous radiative decay. Since spontaneous decay leads only to transitions to lower-lying levels (unlike collisional excitation) truncation of the bound-state Hilbert space does not introduce errors and thus allows for an exact solution within the Born-Markov (i.e., Wigner-Weiskopf [6]) approximation by directly integrating the Lindblad equation.

We consider a highly charged hydrogenic ion, Kr^{35+}, in the vacuum. The only interaction with the environment is the coupling to the vacuum fluctuations of the radiation field manifesting itself in two ways: the coupling driven by this interaction is the spontaneous radiative decay of the electron from an excited state and also the modification of the eigenenergies of the system by the Lamb shift [13,14]. Since radiative decay is an exothermic process, i.e., the final state energy of the electron is always below its initial energy, the Hilbert space necessary for a representation of all possible final states is restricted. For example, the time evolution of an electron initially in the $4p$ state is completely represented in the Hilbert space covering the first four shells of the electronic states rendering the unitary system within a finite Hilbert space $\mathbb{H}_S$, as is schematically shown in Fig. 2(a).

We can now test the nonunitary QTMC evolution by arbitrarily dividing this finite system into two subspaces consisting of, e.g., the third and fourth shell representing $\mathbb{P}$ containing the initial state $4p$ [Fig. 2(b)]. Accordingly, the complement $\mathbb{Q}$ contains the first and second shell. This system features now a net flux from $\mathbb{P}$ to $\mathbb{Q}$ (e.g., by a direct Ly_{γ} transition or a radiative cascade) and is thus open with respect to probability flux. Moreover, there is no probability flowing back from the energetically lower-lying complement $\mathbb{Q}$ to the subspace $\mathbb{P}$. Therefore, for this model system, a properly constructed nonunitary QTMC should exactly reproduce the results from the full unitary simulation of the whole system for any observables in $\mathbb{P}$.

Using the dipole approximation $\langle\alpha|\vec{\nabla}_{\vec{r}}|\beta\rangle = \omega_{\beta\alpha}\langle\alpha|\vec{r}|\beta\rangle$ with $\omega_{\beta\alpha} = \omega_{\beta} - \omega_{\alpha}$ we obtain the transition operator S for the radiative (r) decay as

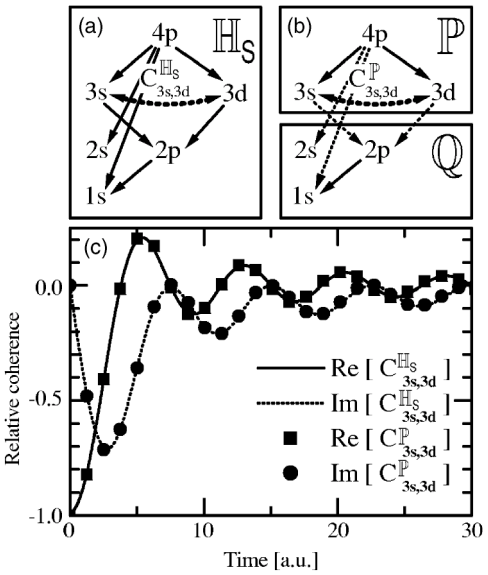

FIG. 2. Test model for a free Kr^{35+} ion under the influence of radiative decay only. (a) Full Hilbert space $\mathbb{H}_S$ with the initial state $4p$. (b) Decomposition into the subspace $\mathbb{P}$ and the complement $\mathbb{Q}$. (c) Comparison of the real and imaginary parts of the relative coherence between the $3s_{1/2,1/2}$ and the $3d_{3/2,1/2}$ states calculated exactly for the entire Hilbert space $\mathbb{H}_S$ ($C^{\mathbb{H}_S}_{3s,3d}$) and using the nonunitary reduction for the subspace $\mathbb{P}$ ($C^{\mathbb{P}}_{3s,3d}$).

$$S_{\alpha\beta}^{(r)}(\mathfrak{J}) = \frac{2}{\sqrt{3c^3}}\omega_{\beta\alpha}^{3/2}\langle\alpha|r_{\mathfrak{J}}|\beta\rangle\theta(\omega_{\beta\alpha}), \tag{3.10}$$

where the index $\mathfrak{J}$ indicates the polarization of the emitted photon. The unperturbed Hamiltonian of the system including relativistic corrections is

$$H_S = -\nabla_r^2/2 - Z_p/r + \Delta H_{rel}, \tag{3.11}$$

where ΔH_{rel} represents relativistic and Lamb shift corrections [5]. The transition operator $S_{\alpha\beta}^{(r)}(\mathfrak{J})$ is defined in the entire Hilbert space $\mathbb{H}_S$ of the electronic states of a hydrogenic atom. By allowing the state indices α and β to cover only the subspace $\mathbb{P}$ we obtain $S_{\alpha\beta}^{(r)\mathbb{P}}(\mathfrak{J}) = S_{\alpha\beta}^{(r)}(\mathfrak{J})$. The construction of the decay operators is straightforward,

$$\Gamma_{\alpha\beta}^{\mathrm{PP}} = \sum_{\nu\in\mathbb{P}}\sum_{\mathfrak{J}} S_{\alpha\nu}^{(r)\dagger}(\mathfrak{J})S_{\nu\beta}^{(r)}(\mathfrak{J}), \tag{3.12}$$

$$\begin{aligned}\Gamma_{\alpha\beta}^{\mathbb{P}} &= \sum_{\gamma\in(\mathbb{P}\oplus\mathbb{Q})}\sum_{\mathfrak{J}} S_{\alpha\gamma}^{(r)\dagger}(\mathfrak{J})S_{\gamma\beta}^{(r)}(\mathfrak{J}) \\ &= \Gamma_{\alpha\beta}^{\mathrm{PP}} + \sum_{\gamma\in(\mathbb{Q})}\sum_{\mathfrak{J}} S_{\alpha\gamma}^{(r)\dagger}(\mathfrak{J})S_{\gamma\beta}^{(r)}(\mathfrak{J}),\end{aligned} \tag{3.13}$$

where the complete Hilbert space $\mathbb{H}_S = \mathbb{P}\oplus\mathbb{Q}$ is represented as a direct sum over the subspace $\mathbb{P}$ and the complement $\mathbb{Q}$.

In Fig. 2(c) we show the time evolution of the reduced density matrix starting initially from a $4p$ state. A remarkable and often overlooked aspect of the radiative decay is that unless the wave packet is projected, i.e., a measurement is taken to determine the state of the emitted photon, the spontaneous decay generates a partially coherent superposition of

states. Only the subsequent feeding and radiative decay of these states leads to dephasing and to decoherence. The different eigenenergies of the final states result in a rotation of the relative complex phase angle as $\exp(-i\omega_{\alpha\beta}t)$ with the time constant $T_{\alpha\beta}^{\text{dephase}}=2\pi/|\omega_{\alpha\beta}|$ which is 7.2 a.u. for the $3s_{1/2,1/2}-3d_{3/2,1/2}$ relative coherence depicted in Fig. 2(c). The latter is defined as

$$C_{\alpha\beta}(t)=\frac{\sigma_{\alpha\beta}(t)}{\sqrt{\sigma_{\alpha\alpha}(t)\sigma_{\beta\beta}(t)}} \tag{3.14}$$

for $\alpha=3s_{1/2,1/2}$ and $\beta=3d_{3/2,1/2}$. Because of $|\sigma_{\alpha\beta}|\leqslant\sqrt{\sigma_{\alpha\alpha}\sigma_{\beta\beta}}$, the absolute magnitude of the relative coherence, $|C_{\alpha\beta}|$, takes values in the interval $0\leqslant|C_{\alpha\beta}|\leqslant 1$. $|C_{\alpha\beta}|=1$ if the system is in a pure state while finite relative coherences smaller than 1 imply that the system is in a partially coherent state.

The near-perfect agreement between the exact result calculated in $\mathbb{H}_S$ and the one calculated with the nonunitary QTMC method employing the split into the $\mathbb{P}$ and $\mathbb{Q}$ subspaces demonstrates the validity of the nonunitary dynamics in $\mathbb{P}$. Clearly this level of agreement is, in part, due to the fact that the back coupling from $\mathbb{Q}$ to $\mathbb{P}$, which is neglected in our approach, vanishes exactly in this problem.

IV. APPLICATION: EXCITED-STATE EVOLUTION IN FAST HIGHLY CHARGED IONS IN SOLIDS

In this section we will apply the nonunitary QTMC method to atoms in a violent collisional environment. More precisely, we will consider a fast projectile during its passage through a solid. The target solid will be decomposed into two components, i.e., reservoirs. One consists of the ionic cores of the target atoms screened by the surrounding electrons. The interaction with them will lead to phonon excitations in the solid as reservoir degrees of freedom. The second reservoir the projectile interacts with are the electrons of the target resulting in plasmon and single-particle–single-hole excitations of the quasifree-electron gas. This system has been previously investigated within the framework of the quantum transport theory employing the unitary QTMC method. Details of the input used can be found in Ref. [5]. We focus in the following only on those aspects of the theory that require modifications for the present nonunitary formulation.

The Lindblad operator for reservoir of quasifree electrons is given by

$$S_{\alpha\beta}^{(e)}(\vec{k})=\sqrt{\frac{8\pi}{k^2}\text{Im}\left[\frac{-1}{\epsilon(\vec{k},\omega_{\beta\alpha}-\vec{k}\cdot\vec{v}_p)}\right]}\theta(\omega_{\beta\alpha}-\vec{k}\cdot\vec{v}_p)\times\langle\alpha|e^{i\vec{k}\cdot\vec{r}}|\beta\rangle \tag{4.1}$$

with the dielectric response function of the electron gas $\epsilon(\vec{k},\omega)$ and $\vec{k}$ representing the momentum transferred in the transition. Using data obtained from photon absorption and electron energy-loss spectroscopy (EELS), the parametrization form of $\epsilon(\vec{k},\omega)$ [15–17] enables us to include in $\epsilon(\vec{k},\omega)$ not only excitations of the valence band but also excitations of inner-shell electrons [18]. Since the projectile moves with a velocity $\vec{v}_p$ through the electron gas, the frequency spectrum of the response is Doppler shifted by $\vec{k}\cdot\vec{v}_p$ introducing a minimum-energy transfer given by the step function θ in Eq. (4.1).

For the interaction with the reservoir of screened ionic cores of the solid,

$$S_{\alpha\beta}^{(c)}(\vec{k}_\perp)=\sqrt{\frac{2\pi n_A}{v_p}}\widetilde{V}_c\left(\vec{k}_\perp+\hat{z}\frac{\omega_{\beta\alpha}}{v_p}\right)\langle\alpha|e^{i[\vec{k}_\perp+\hat{z}(\omega_{\beta\alpha}/v_p)]\cdot\vec{r}}|\beta\rangle, \tag{4.2}$$

with the number density n_A of the ions in the solid and the Fourier transform of the screened Coulomb potential $V_c(\vec{r})=-(Z_T/r)e^{-r/a_{TF}}$, $\widetilde{V}_c(\vec{k})=-(4\pi Z_T)/(k^2+a_{TF}^{-2})$, with the Thomas-Fermi screening length $a_{TF}=0.885Z_T^{-1/3}$ and the nuclear charge of the target atoms, Z_T. The component of the momentum transfer parallel to the projectile velocity k_z is fixed by the requirement $\omega_{\beta\alpha}=\vec{k}\cdot\vec{v}_p$, while the component $\vec{k}_\perp$ specifies the perpendicular momentum transferred.

Both transition operators S [Eqs. (4.1) and (4.2)] can be expressed in the form

$$S_{\alpha\beta}^{(e)}(\vec{k})=f^{(e)}(\omega_{\beta\alpha},\vec{k})\langle\alpha|e^{i\vec{k}\cdot\vec{r}}|\beta\rangle, \tag{4.3a}$$

$$S_{\alpha\beta}^{(c)}(\vec{k}_\perp)=f^{(c)}(\omega_{\beta\alpha},\vec{k}_\perp)\langle\alpha|e^{i[\vec{k}_\perp+\hat{z}(\omega_{\beta\alpha}/v_p)]\cdot\vec{r}}|\beta\rangle \tag{4.3b}$$

with the prefactors $f^{(e)}(\omega_{\beta\alpha},\vec{k})$ and $f^{(c)}(\omega_{\beta\alpha},\vec{k}_\perp)$ given by Eqs. (4.1) and (4.2), respectively. This factorization of the transition operators S will be used below.

The decay operator for core collisions is

$$\Gamma_{\alpha\beta}^{(c)\mathbb{P}}(\vec{k}_\perp)=\sum_{\gamma\in(\mathbb{P}\oplus\mathbb{Q})}S_{\alpha\gamma}^{(c)\dagger}(\vec{k}_\perp)S_{\gamma\beta}^{(c)}(\vec{k}_\perp) \tag{4.4}$$

$$=\Gamma_{\alpha\beta}^{(c)\mathbb{P}\mathbb{P}}(\vec{k}_\perp)+\sum_{\gamma\in\mathbb{Q}}S_{\alpha\gamma}^{(c)\dagger}(\vec{k}_\perp)S_{\gamma\beta}^{(c)}(\vec{k}_\perp), \tag{4.5}$$

where the states α and β are elements of $\mathbb{P}$ and we denoted the partial sum over $\mathbb{P}$ as $\Gamma_{\alpha\beta}^{(c)\mathbb{P}\mathbb{P}}(\vec{k}_\perp)$ [as in Eq. (3.13)]. For the further evaluation of Eq. (4.5) we employ the approximate factorization [Eq. (4.3b)]

$$\Gamma_{\alpha\beta}^{(c)\mathbb{P}}(\vec{k}_\perp)\simeq\Gamma_{\alpha\beta}^{(c)\mathbb{P}\mathbb{P}}(\vec{k}_\perp)+f^{(c)\dagger}(\overline{\omega}_\alpha,\vec{k}_\perp)f^{(c)}(\overline{\omega}_\beta,\vec{k}_\perp)\times\sum_{\gamma\in\mathbb{Q}}\langle\alpha|e^{-i\vec{k}_\alpha(\vec{k}_\perp)\cdot\vec{r}}|\gamma\rangle\langle\gamma|e^{i\vec{k}_\beta(\vec{k}_\perp)\cdot\vec{r}}|\beta\rangle \tag{4.6}$$

with $\vec{k}_\alpha(\vec{k}_\perp)=\vec{k}_\perp+\hat{z}\overline{\omega}_\alpha/v_p$ and $\vec{k}_\beta(\vec{k}_\perp)=\vec{k}_\perp+\hat{z}\overline{\omega}_\beta/v_p$ where we have approximated the energy transfer $\omega_{\alpha\gamma}$ ($\omega_{\beta\gamma}$) by an average excitation energy $\overline{\omega}_\alpha$ ($\overline{\omega}_\beta$) independent on the state γ. The latter is a prerequisite for using the closure relation

$$\sum_{\gamma\in\mathbb{H}_S}\langle\alpha|e^{-i\vec{k}_\alpha(\vec{k}_\perp)\cdot\vec{r}}|\gamma\rangle\langle\gamma|e^{i\vec{k}_\alpha(\vec{k}_\perp)\cdot\vec{r}}|\beta\rangle=\delta_{\alpha\beta}. \tag{4.7}$$

Consequently, we obtain the decay operator $\Gamma^{\mathbb{P}}$,

$$\Gamma_{\alpha\beta}^{(c)\mathbb{P}}(\vec{k}_\perp)\simeq\Gamma_{\alpha\beta}^{(c)\mathbb{P}\mathbb{P}}(\vec{k}_\perp)+|f^{(c)}(\overline{\omega}_\alpha,\vec{k}_\perp)|^2\times\left(\delta_{\alpha\beta}-\sum_{\gamma\in\mathbb{P}}\langle\alpha|e^{-i\vec{k}_\alpha(\vec{k}_\perp)\cdot\vec{r}}|\gamma\rangle\langle\gamma|e^{i\vec{k}_\alpha(\vec{k}_\perp)\cdot\vec{r}}|\beta\rangle\right), \tag{4.8}$$

valid for all diagonal elements ($\alpha=\beta$) and the most impor-

tant subset of off-diagonal elements $\alpha \neq \beta$ between nearly degenerate states with $\omega_\alpha = \omega_\beta$, $\overline{\omega}_\alpha = \overline{\omega}_\beta$, and consequently $\vec{k}_\alpha(\vec{k}_\perp) = \vec{k}_\beta(\vec{k}_\perp)$.

With the closure approximation (4.7) we reduce the infinite sum over the full Hilbert space $\mathbb{H}_S$ in Eq. (4.4) to sums in the finite Hilbert subspace $\mathbb{P}$ of the system. The price we have to pay is the approximation of the energy transfer $\omega_{\alpha\gamma}$ ($\omega_{\beta\gamma}$) by an average excitation energy $\overline{\omega}_\alpha$ ($\overline{\omega}_\beta$) so that the prefactor can be pulled out of the sum over $\gamma \in \mathbb{Q}$ in Eq. (4.6). A proper choice of $\overline{\omega}_\alpha$ ($\overline{\omega}_\beta$) determines significantly the quality of the closure approximation for $\Gamma^{(c)\mathbb{P}}(\vec{k}_\perp)$. For fast collisional excitations in a solid it has been shown [19] that the generalized oscillator strength distribution ("Bethe ridge") peaks around the ionization threshold, i.e., a highly excited state or a low-lying continuum state. This consideration suggests the choice of the ionization energy for the average excitation energy $\overline{\omega}_\alpha = \epsilon_\alpha$, i.e., $\omega_\gamma \to 0$. The total transition matrix $\Gamma^{(c)\mathbb{P}}_{\alpha\beta}$ is obtained from Eq. (4.8) by the integration

$$\Gamma^{(c)\mathbb{P}}_{\alpha\beta} = \frac{1}{(2\pi)^3} \int d^2k_\perp \Gamma^{(c)\mathbb{P}}_{\alpha\beta}(\vec{k}_\perp). \tag{4.9}$$

For off-diagonal elements between strongly nondegenerate states ($\epsilon_\alpha \neq \epsilon_\beta$) we invoke the additional approximation that the degree of coherence $\Gamma^{(c)}_{\alpha\beta}/\sqrt{\Gamma^{(c)}_{\alpha\alpha}\Gamma^{(c)}_{\beta\beta}}$ is the same for $\Gamma^{(c)\mathbb{PP}}_{\alpha\beta}$ and $\Gamma^{(c)\mathbb{P}}_{\alpha\beta}$. We thus calculate $\Gamma^{(c)\mathbb{P}}_{\alpha\beta}$ by rescaling $\Gamma^{(c)\mathbb{PP}}_{\alpha\beta}$ for $\alpha \neq \beta$ as

$$\Gamma^{(c)\mathbb{P}}_{\alpha\beta} = \Gamma^{(c)\mathbb{PP}}_{\alpha\beta} \sqrt{\frac{\Gamma^{(c)\mathbb{P}}_{\alpha\alpha}\Gamma^{(c)\mathbb{P}}_{\beta\beta}}{\Gamma^{(c)\mathbb{PP}}_{\alpha\alpha}\Gamma^{(c)\mathbb{PP}}_{\beta\beta}}}. \tag{4.10}$$

Note, however, that because of the rapid decoherence between strongly nondegenerate states this additional approximation has little influence on the numerical results.

Similarly, the decay operator for scattering at the electron gas is calculated as

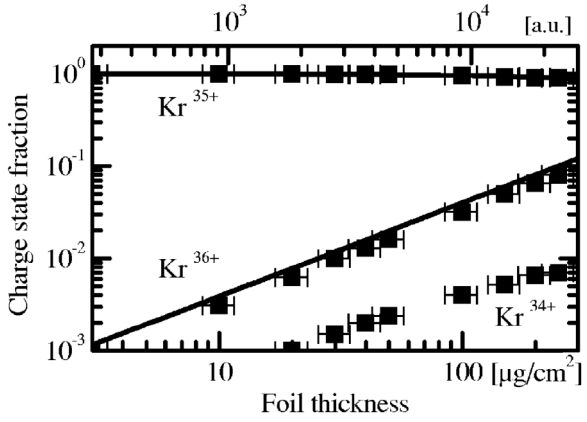

FIG. 3. Charge state fraction of a $Kr^{35+}(1s)$ ion in transport through amorphous carbon at a velocity of $v_p = 47$ a.u. as a function of foil thickness. Symbols are experimental data from Ref. [24] and lines show results of the nonunitary QTMC simulation. The thickness of 1 $\mu g/cm^2$ of amorphous carbon with a density of 2 g/cm^3 corresponds to a propagation length of 92 a.u.

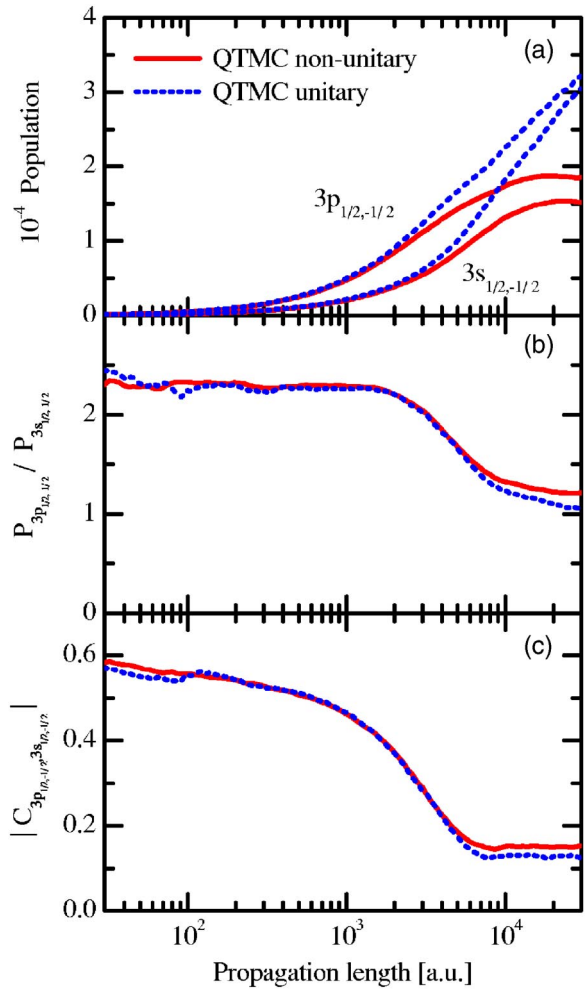

FIG. 4. Evolution of selected populations and coherences of the internal state of a Kr^{35+} ion traversing an amorphous carbon foil with velocity $v_p = 47$ a.u. as a function of propagation length. The system is initially prepared in the $1s$ ground state. We compare results of the nonunitary simulation (solid lines) with results obtained in a unitary simulation (dotted lines) with $n_c = 4$. (a) Populations of the $3s_{1/2,-1/2}$ and $3p_{1/2,-1/2}$ states, (b) ratio of these populations, and (c) relative coherence between these two states.

$$\Gamma^{(e)\mathbb{P}}_{\alpha\beta}(\vec{k}) = \sum_{\gamma \in (\mathbb{P}\oplus\mathbb{Q})} S^{(e)\dagger}_{\alpha\gamma}(\vec{k}) S^{(e)}_{\gamma\beta}(\vec{k})$$

$$\simeq \Gamma^{(e)\mathbb{PP}}_{\alpha\beta}(\vec{k}) + f^{(e)\dagger}(\overline{\omega}_\alpha, \vec{k}) f^{(e)}(\overline{\omega}_\beta, \vec{k}) \tag{4.11}$$

$$\times \sum_{\gamma \in \mathbb{Q}} \langle \alpha | e^{-i\vec{k}\cdot\vec{r}} | \gamma \rangle \langle \gamma | e^{i\vec{k}\cdot\vec{r}} | \beta \rangle \tag{4.12}$$

with the transition operator $S^{(e)}_{\alpha\beta}(\vec{k})$ specified in Eq. (4.1). Unlike the corresponding equation for core collisions (4.6), the momentum transfers $\vec{k}$ of the boost operators in Eq. (4.12) are identical and we can thus apply the closure approximation without restricting the resulting $\Gamma^{(e)\mathbb{P}}_{\alpha\beta}(\vec{k})$ to near-degenerate states with $\epsilon_\alpha = \epsilon_\beta$. The total transition matrix $\Gamma^{(c)\mathbb{P}}_{\alpha\beta}$ is then obtained by the integration

$$\Gamma^{(e)\mathbb{P}}_{\alpha\beta} = \frac{1}{(2\pi)^3}\int d^3k\, \Gamma^{(e)\mathbb{P}}_{\alpha\beta}(\vec{k}) \tag{4.13}$$

without any further approximation.

V. NUMERICAL RESULTS

The collision system we are investigating in the following is the transport of a $Kr^{35+}(1s)$ ion with a velocity of 47 a.u. through amorphous carbon foils of varying thickness, corresponding to varying evolution times. The Hamiltonian of the system is given by Eq. (3.11), however, with interaction with the wake field induced by the projectile ion [20] included. For small distances from the projectile nucleus this wake of density fluctuations creates, to leading order, a linear electric field that causes Stark splitting of the projectile electronic eigenstates. A more detailed description of H_S can be found in Ref. [10].

To explore the effect of our nonunitary QTMC method we present two different simulations of the transport. First, we consider the nonunitary QTMC method within the subspace $\mathbb{P}$ spanned by the hydrogenic basis set with the quantum numbers n, l, j, and m_j. We label the resulting time evolved nonunitary density matrix as $\sigma^{\mathrm{NU}}(t)$. To be consistent with our previous work [5] we choose $\mathbb{P}$ as the Hilbert space represented by the first four shells of the hydrogenic basis set ($n_c=4$) limiting the size of $\sigma^{\mathrm{NU}}(t)$ to 60×60 elements. We note, however, that extensions to larger subspaces are computationally feasible. Increasing the dimension of $\mathbb{P}$, for example to 182×182 (corresponding to $n_c=6$), does not significantly modify the results. The time evolution is governed by the decay operator $\Gamma^{\mathbb{P}}$ in the effective Hamiltonian $H^{\mathbb{P}}_{eff}$ [Eq. (3.6)]. For comparison we use the unitary QTMC method involving $\Gamma^{\mathbb{PP}}$ while leaving all other parameters unchanged. The resulting unitary density matrix will be denoted by $\sigma^{U}(t)$. Since in this work we are dealing with the passage of fast projectiles through thin targets we can treat the velocity of the projectile nucleus as constant and neglect the slowing down of the projectile. We use time t in the projectile rest frame and distance d in the laboratory frame

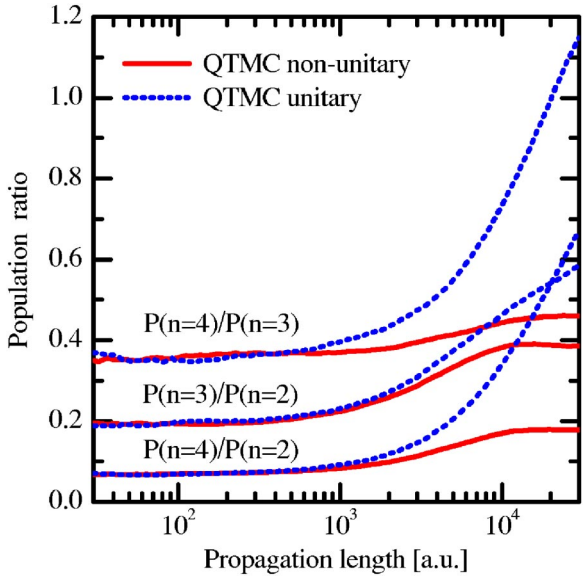

FIG. 5. Evolution of shell population ratios as a function of propagation length for the nonunitary QTMC (solid lines) and a unitary QTMC simulation (dotted lines) with $n_c=4$.

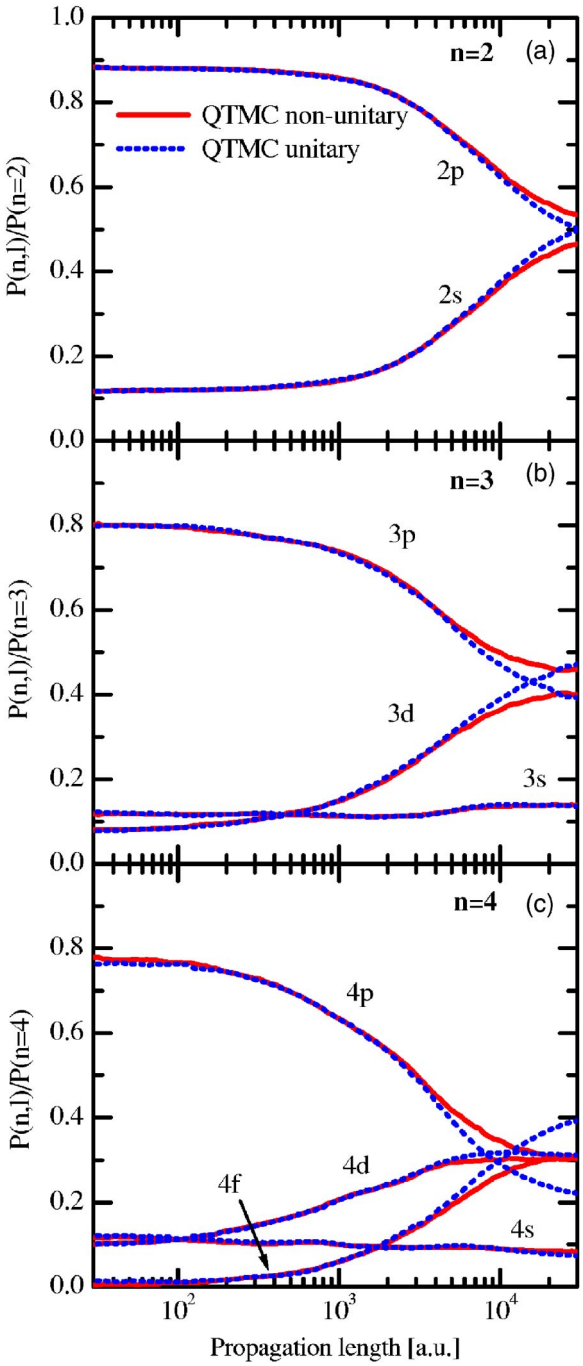

FIG. 6. Evolution of relative populations of Kr^{35+} states as a function of propagation length for the full nonunitary QTMC (solid lines) and a unitary QTMC simulation (dotted lines) with $n_c=4$. Results are shown for different principal quantum numbers n and angular momenta l. The populations are normalized to the overall probability in the corresponding shell. (a) $P(n=2,l)$ for $n=2$, (b) $P(n=3,l)$ for $n=3$, and (c) $P(n=4,l)$ for $n=4$.

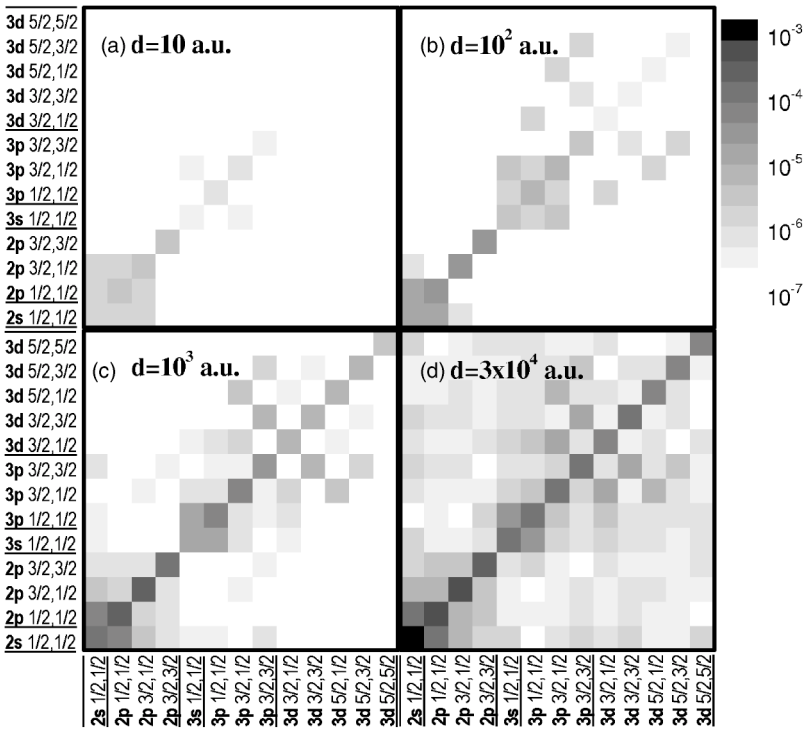

FIG. 7. Reduced density matrix of a Kr^{35+} ion in transport through amorphous carbon at a velocity of $v_p=47$ a.u. at various propagation lengths. (a) $d=10$ a.u., (b) $d=10^2$ a.u., (c) $d=10^3$ a.u., and (d) $d=3\times10^4$ a.u. Absolute magnitude of excited-states matrix elements $|\sigma_{ij}^{NU}(d)|$ from $n=2$ and $n=3$ involving $m_j>0$ are shown.

interchangeably with $d(t=0)=0$ at the entrance of the foil and $d(t)=v_p t/\sqrt{1-(v_p/c)^2}$.

Figure 3 shows that while the ionized fraction of Kr^{35+} ions is small for thin foils, for the largest foil thickness used in the experiment about 10% of the projectile ions are fully stripped. This fraction is an approximate measure of the loss of probability of the one-electron bound-state Hilbert space due to transitions to the continuum. More precisely, all high-lying bound states with $n>n_c$ also belong to $\mathbb{Q}$ increasing this fraction somewhat. In addition, capture of a second electron leading to the formation of Kr^{34+} would represent a further loss channel corresponding to the transition from a one-electron to a two-electron Hilbert space. Figure 3 indicates that this is for the system under consideration a slow process leading to only 1% Kr^{34+} for the thickest foil and is neglected in the following. Loss due to ionization dominates and has motivated our investigation of nonunitary transport. By comparing the experimental findings with the results of the nonunitary QTMC we find that the trace of the density matrix, $\mathrm{Tr}[\sigma^{NU}(d)]$ and $1-\mathrm{Tr}[\sigma^{NU}(d)]$, agree well with the charge state probability for Kr^{35+} and Kr^{36+}, respectively.

The effect of the nonunitary evolution on individual state populations and coherences is shown in Fig. 4 for the $3s_{1/2,-1/2}$ and $3p_{1/2,-1/2}$ subspace. The most pronounced difference is observed for the populations of these states. While in a unitary calculation the feeding from low-lying states remains dominant even for long propagation lengths, in the nonunitary simulation loss from higher excited states into the complement $\mathbb{Q}$ lead to a depletion and thus to a dynamical equilibrium of the populations shown in Fig. 4(a). Remarkably, the population ratio between states of different angular momenta within the same shell [Fig. 4(b)] is very similar in both calculations, the nonunitary QTMC results showing a slightly higher ratio for thick targets. Also for the relative coherence [Eq. (3.14)] only a slight increase is observed.

By contrast, the shell populations rations $P(n)/P(n')$ show drastic modifications when loss into $\mathbb{Q}$ is taken into account (Fig. 5). For small propagation lengths the ratios between shell populations are controlled by single collisions and remain constant. They are identical in the unitary and nonunitary QTMC simulation. In the multiple collision regime the unitary simulation accumulates the electron probability in the higher-lying shells while in the nonunitary simulation the ratios approach saturation. In this regime the flow of probability among states in $\mathbb{P}$ balances the flow of flux from $\mathbb{P}$ to $\mathbb{Q}$ and back to the 1*s* state.

The relative subshell populations of states with different angular momenta within a shell as a function of propagation length agree for a unitary and a nonunitary QTMC calculation for short distances (Fig. 6). However, differences become noticeable at large distances. Relative to the nonunitary QTMC result the unitary transport enhances the probability for higher angular momentum states.

The buildup and decay of coherences is most directly observed in the reduced density matrix $|\sigma_{ij}^{NU}(d)|$, which displays, on one hand, the excitation to excited states in the diagonal elements $\sigma_{ii}^{NU}(d)$ and, on the other hand, the coherences in the off-diagonal elements of $\sigma_{ij}^{NU}(d)$ $(i\neq j)$. The absolute magnitude of the elements of σ^{NU} for excited states is given in Fig. 7 while the matrix of relative coherences is shown in Fig. 8 for different propagation distances *d*. While Figs. 7(a) and 7(b) reflect the excitation by single collisions, Figs. 7(c) and 7(d) reflect the multiple collision regime, where we can observe not only the initially generated coherences by excitation from the 1*s* ground state but also coherences generated by deexcitation. Coherences most robust against decoherence and still visible after a propagation length of 3×10^4 a.u. ($\sim$15 fs) are intrashell coherences between different angular momentum states.

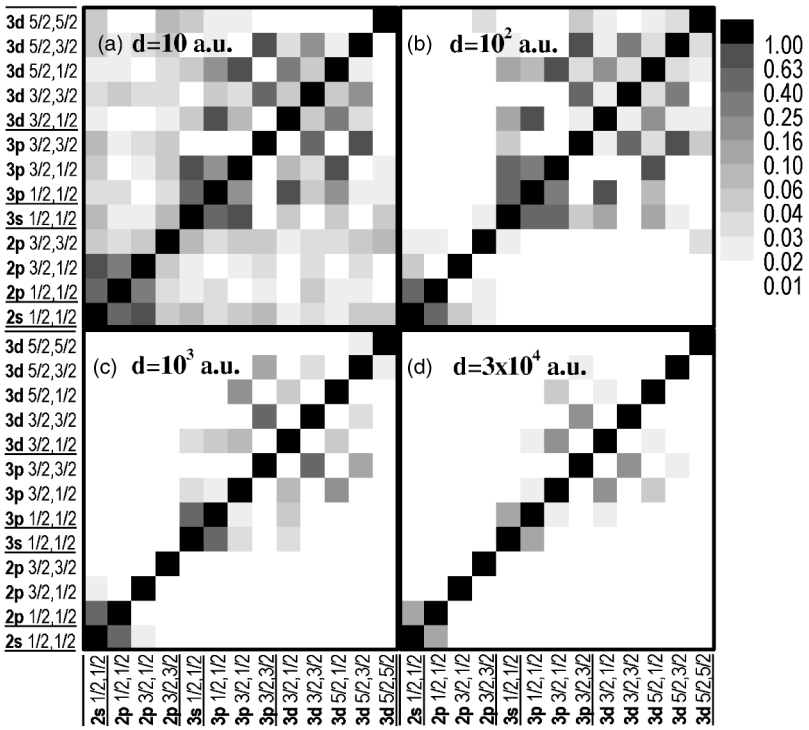

FIG. 8. Relative coherences $|C_{ij}^{NU}(d)|$ of the reduced density matrix of a Kr^{35+} ion in transport through amorphous carbon at a velocity of $v_p = 47$ a.u. at various propagation lengths. (a) $d = 10$ a.u., (b) $d = 10^2$ a.u., (c) $d = 10^3$ a.u., and (d) $d = 3 \times 10^4$ a.u. Only matrix elements from $n = 2$ and $n = 3$ involving $m_j > 0$ are shown.

The matrix of relative coherences [Eq. (3.14)] displayed in Fig. 8 shows the gradual shift and decay of coherences as a function of propagation distance (or foil thickness). The intrashell coherences between the $2s$ and $2p$ states survive longest. Two mechanisms are destroying coherence (i.e., decoherence): dephasing and dissipation. The characteristic time of dephasing between two states is mainly determined by the inverse of the difference of their eigenenergies as

$$T_{\alpha\beta}^{\text{dephase}} = 2\pi/|\omega_{\alpha\beta}|. \tag{5.1}$$

Table I lists the path length for dephasing, d^{dephase}, the projectile travels during the dephasing time $T_{\alpha\beta}^{\text{dephase}}$ for intrashell states (α, β). The point to be noted is that most of the nonvanishing coherences survive for longer than predicted by Eq. (5.1). The reason is that as long as the primary source, the $1s$ ground state, is still populated, the excited-state coherences get replenished and a transient dynamical equilibrium is established for coherences.

Figures 7 and 8 do not present direct information on the phase of the density-matrix element σ_{ij}^{NU}. We therefore display in Figs. 9 and 10 the trajectories in the complex plane of a selected set of density matrix elements with snapshots taken at different propagation distances. While coherences shown in Fig. 9 are destroyed primarily by dephasing, in Fig. 10 dissipation in the dominant decoherence mechanism. For a better comparison we rescale in Fig. 9 the propagation distance by the corresponding dephasing distance d^{dephase} for each coherence separately. Starting at the origin, the selected elements of the reduced density matrix $\sigma_{ij}^{NU}(d)$ [Figs. 9(a)–9(c)] evolve counterclockwise in the complex plane with increasing propagation path. This subset has in common that the buildup of coherence occurs already in the single-collision regime. These elements approximately complete one circle in the complex plane after each multiple of d^{dephase}. The shift, i.e., the fact that after a 2π rotation the trajectory does not exactly return to its starting point, signifies the effect of multiple collisions and radiative decay during further transport. The element $\sigma_{2s_{1/2,1/2},2p_{3/2,1/2}}$ (dashed line in Fig. 9) with the shortest dephasing path $d^{\text{dephase}} = 100$ a.u. is least affected whereas $\sigma_{3p_{3/2,3/2},3d_{5/2,3/2}}$ (solid line) with a ten times longer dephasing path is strongly perturbed. Multiple scattering and dissipation manifests itself in a shift

TABLE I. Dephasing length $d_{\alpha\beta}^{\text{dephase}}$ in a.u. for a Kr^{35+} ion traveling with a speed of 47 a.u. during the time $T_{\alpha\beta}^{\text{dephase}} = 2\pi/|\omega_{\alpha\beta}|$ for intrashell combinations of hydrogenic eigenstates with the unperturbed Hamiltonian specified in Eq. (3.11).

$\mathbf{n}=2$	$\alpha=2s_{1/2}$	$2p_{1/2}$		
$\beta=2p_{3/2}$	110	107		
$2p_{1/2}$	4954			
$\mathbf{n}=3$	$\alpha=3s_{1/2}$	$3p_{1/2}$	$3p_{3/2}$	$3d_{3/2}$
$\beta=3d_{5/2}$	274	270	1118	1125
$3d_{3/2}$	363	355	178224	
$3p_{3/2}$	363	356		
$3p_{1/2}$	16547			
$\mathbf{n}=4$	$\alpha=4s_{1/2}$	$4p_{3/2}$	$4d_{5/2}$	
	$\alpha=4p_{1/2}$	$4d_{3/2}$	$4f_{5/2}$	
$\beta=4f_{7/2}$	580	1780	5369	
$4d_{5/2},4f_{5/2}$	651	2663		
$4p_{3/2},4d_{3/2}$	861			

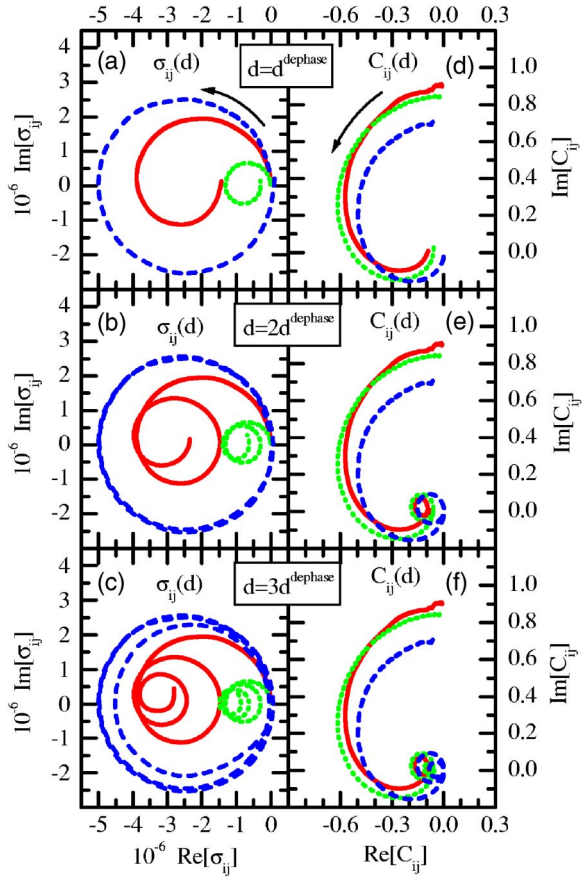

FIG. 9. Evolution of selected elements of the density matrix σ_{ij}^{NU} of a Kr^{35+} ion in transport through amorphous carbon at a velocity of $v_p=47$ a.u. for different propagation lengths in the complex plane. The left column, i.e., (a), (b), and (c), shows off-diagonal elements of the density matrix σ_{ij}^{NU} while the right column, i.e., (d), (e), and (f), shows the relative coherence C_{ij}^{NU}, i.e., the off-diagonal elements σ_{ij}^{NU} normalized to the population of the involved states [$\sigma_{i,i}^{NU}$ and $\sigma_{j,j}^{NU}$ according to Eq. (3.14)]. The maximum propagation length of each coherence has been rescaled, such that in the first row, (a) and (d), it corresponds to the dephasing length $d^{dephase}$ shown in Table I. For the second row, (b) and (d), $d=2d^{dephase}$ and for the third row, (c) and (f), $d=3d^{dephase}$. Solid lines: $\sigma^{NU}_{3p_{3/2,3/2},3d_{5/2,3/2}}$; dotted lines: $\sigma^{NU}_{3p_{1/2,1/2},3d_{3/2,1/2}}$; dashed lines: $\sigma^{NU}_{2s_{1/2,1/2},2p_{3/2,1/2}}$.

of the circle as well as in a shrinking radius of the rotation.

The relative coherence $C_{ij}^{NU}(d)$ in Figs. 9(d)–9(f) starts out to be purely imaginary as expected in a single collision when the Born approximation holds. Just after one single rotation ($d=d^{dephase}$) the relative coherence approaches the origin of the complex plane indicating very fast decrease in coherence while still performing further revolutions.

In Fig. 10 we selected elements of $\sigma_{ij}^{NU}(d)$ with a long dephasing length ($d^{dephase}$) such that multiple collisions dominate the buildup of coherence and decoherence. We selected four elements of $\sigma_{ij}^{NU}(d)$ that approach a nonvanishing larger (transient) equilibrium value of the relative coherence $|C_{ij}| \geq 0.1$ within the propagation distances studied. Starting at the origin [Fig. 10(a)] the coherences first evolve along circles of different radii [Fig. 10(b)]. Note that in this figure

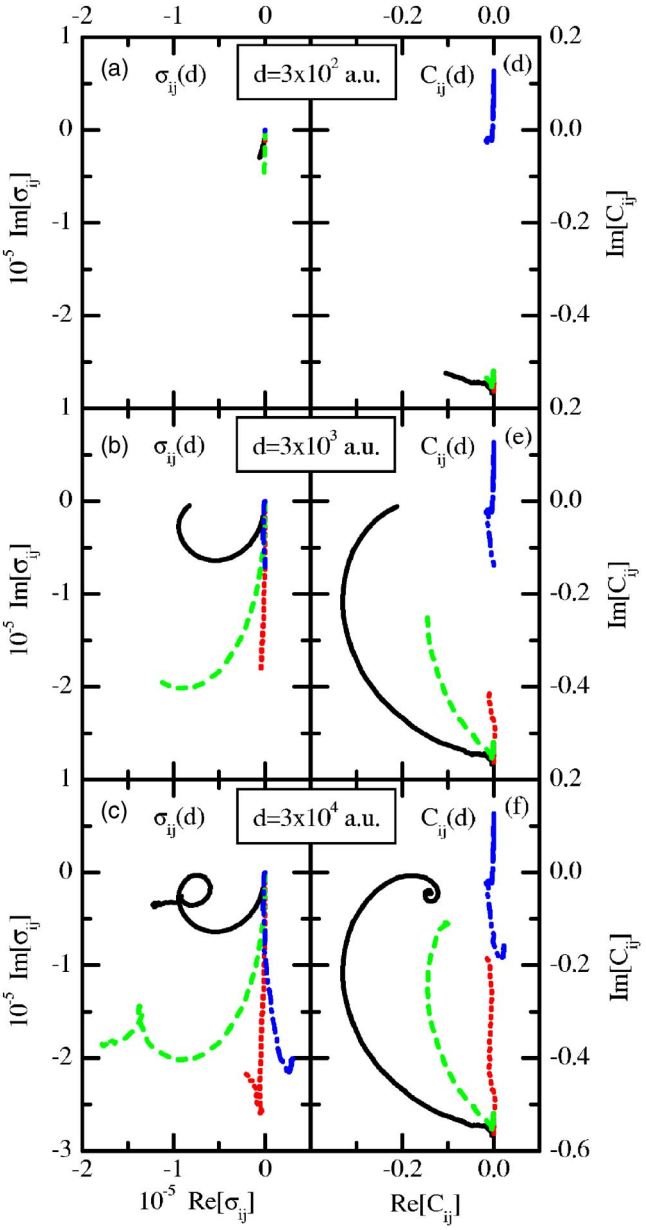

FIG. 10. Evolution of selected elements of the density matrix σ_{ij}^{NU} of a Kr^{35+} ion in transport through amorphous carbon at a velocity of $v_p=47$ a.u. for different maximum propagation lengths in the complex plane. The left column, i.e., (a), (b), and (c), shows off-diagonal elements of the density matrix σ_{ij}^{NU} while the right column, i.e., (d), (e), and (f), shows the relative coherences C_{ij}, i.e., the off-diagonal elements σ_{ij}^{NU} normalized to the population of the involved states [$\sigma_{i,i}^{NU}$ and $\sigma_{j,j}^{NU}$ according to Eq. (3.14)]. Solid lines: $\sigma^{NU}_{2s_{1/2,1/2},2p_{1/2,1/2}}$; dashed lines: $\sigma^{NU}_{3s_{1/2,1/2},3p_{1/2,1/2}}$; dotted lines: $\sigma^{NU}_{3p_{3/2,3/2},3d_{3/2,3/2}}$; and dot-dashed lines, $\sigma^{NU}_{3p_{3/2,1/2},3d_{3/2,1/2}}$. The results shown in (a)–(c) for $\sigma^{NU}_{2s_{1/2,1/2},2p_{1/2,1/2}}$ (solid lines) have been divided by 10.

(unlike Fig. 9) we have not rescaled the propagation path but show the density matrix for the identical propagation path in each plot ranging from $d=3\times10^2$ a.u. to $d=3\times10^4$. Therefore some elements with relatively short $d^{dephase}$ succeed in almost completing one circle while others with a long $d^{dephase}$ still evolve almost tangentially. Multiple collisions and radia-

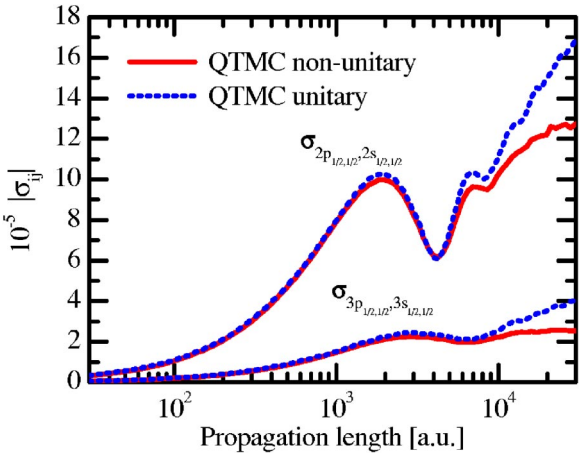

FIG. 11. Comparison of selected coherences of a Kr^{35+} ion in transport through amorphous carbon at a velocity of $v_p=47$ a.u. as a function of propagation length. We show absolute magnitude $|\sigma_{ij}^{U,NU}|$ of coherences between s and p states for $n=2$ and $n=3$ obtained by a nonunitary QTMC (solid lines) and by a unitary QTMC simulation (dotted lines) with $n_c=4$.

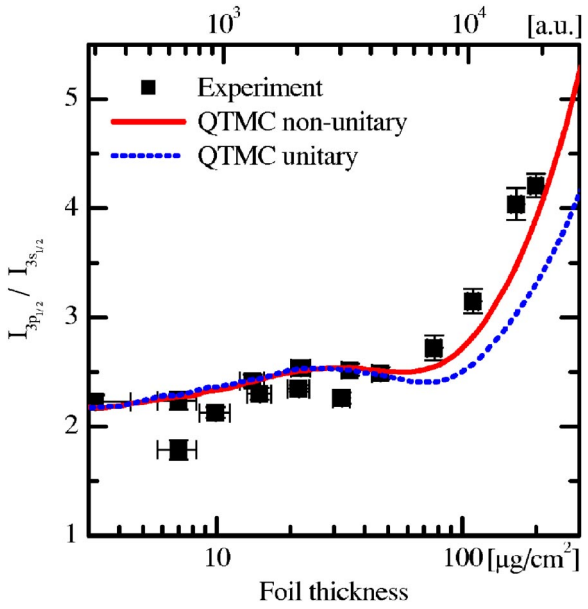

FIG. 12. Relative line emission intensities $I_{3p_{1/2}}/I_{3s_{1/2}}$ resulting from the transmission of a $Kr^{35+}(1s)$ ion through amorphous carbon at a velocity of 47 a.u. as a function of target thickness. Symbols are experimental data from Ref. [24], the solid line shows the result of the nonunitary QTMC simulation and the dotted line represents results obtained by a unitary QTMC simulation with $n_c=4$.

tive decay (i.e., dissipation) completely distort this circular motion for long propagation paths in Fig. 10(c). The long-time behavior of these elements of $\sigma_{ij}^{NU}(d)$ mimics Brownian motion in the complex plane. Since these coherences are most sensitive to an accurate theoretical description, they provide a test for our approach.

It is important to note that the diagonal as well as the off-diagonal elements of σ_{ij}^{NU} are very sensitive to the competition between gain and loss. It is the contribution from the loss into the complement $\mathbb{Q}$, included in the present calculation, that significantly changes σ_{ij}^{NU} in the region where a transient equilibrium persists. The diagonal elements of σ_{ii}^{NU}, the population probabilities, are clearly very different from a unitary σ_{ij}^{U} as discussed before. Likewise, the off-diagonal elements of $\sigma_{ij}^{U}(d)$ do not reach an equilibrium (Fig. 11) unlike those of $\sigma_{ij}^{NU}(d)$.

We conclude this section by presenting a comparison with the experiment that originally stimulated our investigation. The experiment we compare with has been performed at GANIL (Grand Accélérateur National d'Ions Lourde) on the LISE (Ligne d'Ions Super Epluchés) facility. The projectiles used were hydrogenic Kr^{35+} at an energy of 60 MeV/amu corresponding to a collision velocity of $v_p=47$ a.u. The initial state of transport is the ground state Kr^{35+} $(1s)$ in vacuum, we employ a sudden approximation at the foil entrance at which the terms in the Hamiltonian referring to the carbon foil are switched on. Likewise, we project onto atomic final states in vacuum at the exit surface invoking, again, a sudden approximation. Using high-resolution high-transmission Bragg-crystal spectrometers the emitted photons of the Balmer α lines have been measured as a function of foil thickness [10]. The intensities of the emitted Balmer α lines (transitions from $n=3$ to $n=2$) give a measure of the population of the corresponding electronic state of the projectile during the time evolution for states with $n=3$. There are two important details to be considered. First, the line intensities measured are integrated over the whole passage of the projectile through the foil and after exiting it. Therefore the spatial information can only be obtained by repeating the measurement using targets with different thickness. Second, the contributions to a given Balmer line is not only determined by the population collisionally excited to the initial state of this radiative transition but also from all higher excited states feeding this state during the radiative cascade. Details are described in Ref. [10]. In order to correct for the cascade contribution from $n>4$ states, we extrapolate the quantum n,l,m distributions to higher n levels using scaling properties drawn from classical transport theory (CTT) [18,21–23]. We have shown that for high principal quantum numbers n the solution of the NLSSE in Eq. (2.7) reduces to a linear Schrödinger equation for quasifree electrons. For high n only collisional interactions are contributing while radiative decay can be neglected on the time scale considered. We apply the same extrapolation correction to both the unitary and nonunitary QTMC calculation.

In Fig. 12 we compare the experimental intensity ratio $I_{3p_{1/2}}/I_{3s_{1/2}}$ with results obtained with the nonunitary QTMC calculation and with results form a unitary QTMC simulation as a function of target thickness. The nonunitary approach clearly improves the intensity ratio in the regime of multiple collisions for thicker targets and leads to much better agreement with the experimental findings.

VI. SUMMARY

We have introduced a generalized Lindblad master equation for the description of the time evolution of a subspace of the reduced density matrix that allows for the flow of prob-

ability out of the truncated Hilbert space. We have developed the corresponding generalized nonunitary quantum trajectory Monte Carlo method solving this Lindblad master equation and have implemented it for the transport of a fast highly charged hydrogenic ion through a solid.

We have calculated the time evolution of the internal electronic state of a Kr^{35+} ion during transport through carbon with the generalized nonunitary quantum trajectory Monte Carlo method. We find that inclusion of loss processes via a nonunitary formulation of transport leads to a modification of coherences and not just to a change of excited-state populations. The good agreement with experimentally obtained intensity ratios of emitted photons underlines the need for a nonunitary treatment of this transport problem and indicates the validity of our approach for such a complex system.

One conceptual shortcoming of the present formulation is the lack of the capture channel. While insignificant for the experimental data studied in this work, its inclusion is essential for further applications. Work along these lines is in progress.

ACKNOWLEDGMENTS

This work was supported by the NSF, FWF (Austria), and EU under Contract No. HPRI-CT-2001-50036. C.O.R. acknowledges support by the DCS, OBES, USDOE, managed by UT-Battelle, LLC, under Contract No. DE-AC05-00OR22725.

APPENDIX: CORRESPONDENCE OF QTMC AND LINDBLAD FORM IN A NONUNITARY SYSTEM

In this Appendix we briefly show the correspondence of the solution of the QTMC method with the solution of the Lindblad master equation. Our analysis applies to both the unitary and nonunitary QTMC methods. The important point is that only the short-time behavior of the solution enters. The continuous time evolution operator from Eq. (3.4) can be expanded using the Taylor series $e^{-iH_{\rm eff}^{\rm P,PP}dt}=1-iH_{\rm eff}^{\rm P,PP}dt+O(dt^2)$ up to first order in dt as

$$U_{\rm cont}^{\eta}(t+dt,t)|\Psi^{\eta}(t)\rangle = \||\Psi^{\eta}(t)\rangle\| \times\frac{(1-iH_{\rm eff}^{\rm P}\,dt)|\Psi^{\eta}(t)\rangle}{[\langle\Psi^{\eta}(t)|(1+iH_{\rm eff}^{\rm PP\dagger}\,dt)(1-iH_{\rm eff}^{\rm PP}\,dt)|\Psi^{\eta}(t)\rangle]^{1/2}}. \tag{A1}$$

By inserting the definition of the effective Hamiltonian [Eq. (3.6)] the denominator of Eq. (A1) simplifies to $(\langle\Psi^{\eta}(t)|1-\Gamma^{\rm PP}dt|\Psi^{\eta}(t)\rangle)^{1/2}$, so that we obtain in first order of dt

$$U_{\rm cont}^{\eta}(t+dt,t)|\Psi^{\eta}(t)\rangle=\left(1-iH_{\rm eff}^{\rm P}\,dt+\frac{1}{2}\langle\Gamma^{\rm PP}\rangle_{t,\eta}\,dt\right)|\Psi^{\eta}(t)\rangle, \tag{A2}$$

using the definition of the expectation value as

$$\langle\Gamma^{\rm PP}\rangle_{t,\eta}=\langle\Psi^{\eta}(t)|\Gamma^{\rm PP}(t)|\Psi^{\eta}(t)\rangle\,/\,\langle\Psi^{\eta}(t)|\Psi^{\eta}(t)\rangle = \langle\Psi^{\eta}(t)|\Gamma^{\rm PP}|\Psi^{\eta}(t)\rangle/\||\Psi^{\eta}(t)\rangle\|^2$$

.

We define a stochastic variable $N_{\vec{k}}^{\eta}(t)$ that counts the number of jumps up to a time t for a given quantum trajectory η and index $\vec{k}$ of the transition. The differential, also called Ito differential, $dN_{\vec{k}}^{\eta}(t)=N_{\vec{k}}^{\eta}(t+dt)-N_{\vec{k}}^{\eta}(t)$, takes for an infinitesimally short time interval dt the value 1 when a jump happened and 0 for no jump for a given quantum trajectory η. Consequently, the product of two Ito differentials for the same time is $dN_{\vec{k}}^{\eta}(t)dN_{\vec{k}'}^{\eta}(t)=\delta_{\vec{k},\vec{k}'}dN_{\vec{k}}^{\eta}(t)$ because only one jump can occur in an infinitesimal short time interval dt.

The change of the wave function $|d\Psi^{\eta}(t)\rangle=-|\Psi^{\eta}(t)\rangle+|\Psi^{\eta}(t+dt)\rangle$ is

$$|d\Psi^{\eta}(t)\rangle=-|\Psi^{\eta}(t)\rangle + \left[\left(\frac{1}{V}\sum_{\vec{k}}dN_{\vec{k}}^{\eta}(t)U_{\rm jump}^{\eta}(\vec{k},t)\right)U_{\rm cont}^{\eta}(t+dt,t) + \left(1-\frac{1}{V}\sum_{\vec{k}}dN_{\vec{k}}^{\eta}(t)\right)U_{\rm cont}^{\eta}(t+dt,t)\right]|\Psi^{\eta}(t)\rangle, \tag{A3}$$

where the second term corresponds to the case when a jump happens in the time interval dt weighted with probabilities $V^{-1}dN_{\vec{k}}^{\eta}(t)$. The continuous time evolution operator is applied to the wave function first and afterwards the jump operator acts on the evolved quantum trajectory. When no jump happens [third term with the complementary probability of $1-V^{-1}\Sigma_{\vec{k}}dN_{\vec{k}}^{\eta}(t)$] only the continuous time evolution contributes via $U_{\rm cont}^{\eta}(t+dt,t)$.

Inserting the explicit form of $U_{\rm cont}^{\eta}(t+dt,t)$ from Eq. (A2) into the last expression [Eq. (A3)] we obtain

$$|d\Psi^{\eta}(t)\rangle=\left[-iH_{\rm eff}^{\rm P}\,dt+\frac{1}{2}\langle\Gamma^{\rm PP}\rangle_{t,\eta}\,dt + \frac{1}{V}\sum_{\vec{k}}dN_{\vec{k}}^{\eta}(t)[U_{\rm jump}^{\eta}(\vec{k},t)-1] + O\left(\frac{1}{V}\sum_{\vec{k}}dN_{\vec{k}}^{\eta}(t)dt\right)\right]|\Psi^{\eta}(t)\rangle. \tag{A4}$$

All terms in Eq. (A4) proportional to $dN_{\vec{k}}^{\eta}(t)dt$ vanish to first order in dt when we take the average over all stochastic realizations of a quantum trajectory. Inserting the definition of $H_{\rm eff}^{\rm P}$ [Eq. (3.6)] into Eq. (A4) we obtain the NLSSE without specifying the $U_{\rm jump}^{\eta}(\vec{k},t)$ and the jump times in $dN_{\vec{k}}^{\eta}(t)$ as

$$|d\Psi^{\eta}(t)\rangle = \left(-iH_S dt - \frac{dt}{2}(\Gamma^{P} - \langle\Gamma^{PP}\rangle_{t,\eta}) + \frac{1}{V}\sum_{\vec{k}} \overline{dN_{\vec{k}}^{\eta}(t)}[U_{\text{jump}}^{\eta}(\vec{k},t) - 1] \right) |\Psi^{\eta}(t)\rangle. \tag{A5}$$

The ansatz made in Eq. (3.5) for the jump operator leads directly to the NLSSE [Eq. (3.7)].

Finally, the differential change of the reduced density matrix for a stochastic realization $d\sigma^{\eta}(t) = |d\Psi^{\eta}(t)\rangle\langle d\Psi^{\eta}(t)|$ is given by

$$d\sigma^{\eta}(t) = -i[H_S, \sigma^{\eta}(t)]dt + \frac{dt}{2}[\Gamma^{P}, \sigma^{\eta}(t)]_{+} + \langle\Gamma^{PP}\rangle_{t,\eta}\sigma^{\eta}(t)dt + \frac{1}{V}\sum_{\vec{k}} \overline{dN_{\vec{k}}^{\eta}(t)}[\langle\Gamma_{\vec{k}}^{PP}\rangle_{t,\eta}^{-1} S^{P}(\vec{k})\sigma^{\eta}(t)S^{P\dagger}(\vec{k}) - \sigma^{\eta}(t)].$$

The generalized Lindblad form of the master equation [Eq. (3.1)] is obtained with the ansatz for the averaged jump time distribution $\overline{dN_{\vec{k}}^{\eta}(t)}$ as shown in Eq. (3.8) as a sum over quantum trajectories $\sigma(t) = N_{traj}^{-1}\sum_{\eta=1}^{N_{traj}}\sigma^{\eta}(t)$.

[1] J. Dalibard, Y. Castin, and K. Molmer, Phys. Rev. Lett. **68**, 580 (1992).
[2] K. Mølmer, Y. Castin, and J. Dalibard, J. Opt. Soc. Am. B **10**, 524 (1993).
[3] R. Dum, P. Zoller, and H. Ritsch, Phys. Rev. A **45**, 4879 (1992).
[4] H. J. Carmichael, Phys. Rev. Lett. **70**, 2273 (1993).
[5] T. Minami, C. O. Reinhold, and J. Burgdörfer, Phys. Rev. A **67**, 022902 (2003).
[6] G. Lindblad, Commun. Math. Phys. **48**, 119 (1976).
[7] G. Lindblad, Rev. Mod. Phys. **10**, 393 (1976).
[8] U. Kleinekathofer, I. Kondov, and M. Schreiber, Phys. Rev. E **66**, 037701 (2002).
[9] I. Kondov, U. Kleinekathofer, and M. Schreiber, J. Chem. Phys. **119**, 6635 (2003).
[10] T. Minami, C. O. Reinhold, M. Seliger, J. Burgdörfer, C. Fourment, E. Lamour, J.-P. Rozet, D. Vernhet, and B. Gervais, Phys. Rev. A **65**, 032901 (2002).
[11] S. Yoshida, S. Watanabe, C. O. Reinhold, and J. Burgdörfer, Phys. Rev. A **60**, 1113 (1999).
[12] C. W. Gardiner and P. Zoller, *Quantum Noise* (Springer, Berlin, 1999).
[13] B. H. Bransden and C. J. Joachain, *Physics of Atoms and Molecules* (Longman Scientific and Technical, Harlow, 1983).
[14] W. R. Johnson and G. Soff, At. Data Nucl. Data Tables **33**, 405 (1985).
[15] C. Martin, E. T. Arakawa, T. A. Callcott, and J. C. Ashley, J. Electron Spectrosc. Relat. Phenom. **35**, 307 (1985).
[16] J. C. Ashley, J. J. Cowan, R. H. Ritchie, V. E. Anderson, and J. Hoelzel, Thin Solid Films **60**, 361 (1979).
[17] J. Ashley, J. Electron Spectrosc. Relat. Phenom. **28**, 177 (1982).
[18] B. Gervais, C. O. Reinhold, and J. Burgdörfer, Phys. Rev. A **53**, 3189 (1996).
[19] M. Inokuti, Rev. Mod. Phys. **43**, 297 (1971).
[20] P. M. Echenique, W. Brandt, and R. H. Ritchie, Phys. Rev. B **33**, 43 (1986).
[21] J. Burgdörfer and J. Gibbons, Phys. Rev. A **42**, 1206 (1990).
[22] C. O. Reinhold, D. G. Arbó, J. Burgdörfer, B. Gervais, E. Lamour, D. Vernhet, and J. P. Rozet, J. Phys. B **33**, L111 (2000).
[23] J. Kemmler, J. Burgdörfer, and C. O. Reinhold, Phys. Rev. A **44**, 2993 (1991).
[24] D. Vernhet, J.-P. Rozet, I. Bailly-Despiney, C. Stephan, A. Cassimi, J.-P. Grandin, and L. J. Dubé, J. Phys. B **31**, 117 (1998).